Research Article

Pulmonary Circulation

Echocardiographic assessment of right ventricular function in experimental pulmonary hypertension

Zhongkai Zhu[1,2,3], Dureti Godana[2,3], Ailing Li[1], Bianca Rodriguez[2,3], Chenxin Gu[5], Haiyang Tang[4,5], Richard D. Minshall[6], Wei Huang[1] and Jiwang Chen[2,3]

[1]Department of Cardiology, The First Affiliated Hospital, Chongqing Medical University, Chongqing, China; [2]Department of Medicine, Division of Pulmonary, Critical Care Medicine, Sleep and Allergy, Department of Medicine; [3]Research Resources Center, Cardiovascular Research Core, University of Illinois at Chicago, Chicago, IL, USA; [4]State Key Laboratory of Respiratory Disease, Guangzhou Institute of Respiratory Disease, First Affiliated Hospital of Guangzhou Medical University, Guangzhou, China; [5]College of Veterinary Medicine, Northwest A&F University, Yangling, Shaanxi, China; [6]Department of Anesthesiology and Pharmacology, University of Illinois at Chicago, Chicago, IL, USA

Abstract

Echocardiography, a non-invasive and cost-effective method for monitoring cardiac function, is commonly used for evaluation and pre-clinical diagnostics of pulmonary hypertension (PH). Previous echocardiographic studies in experimental models of PH are fragmentary in terms of the evaluation of right ventricle (RV) function. In this study, three rodent models of PH: a mouse model of hypoxia-induced PH, a rat model of hypoxia+Sugen induced PH and a rat model of monocrotaline-induced PH, were employed to measure RV fractional area change (RVFAC), RV free wall thickness (RVFWT), pulmonary acceleration time (PAT), pulmonary ejection time (PET), and tricuspid annular plane systolic excursion (TAPSE). We found that, in these models, RVFWT significantly increased, but RVFAC, PAT, or PAT/PET ratios and TAPSE values significantly decreased. Accurate and complete TAPSE patterns were demonstrated in the three rodent models of PH. The RV echocardiography data matched the corresponding invasive hemodynamic and heart histologic data in each model. This serves as a reference study for real-time and non-invasive evaluation of RV function in rodent models of PH using echocardiography.

Keywords

echocardiography, pulmonary hypertension, right ventricle, mice, rats

Date received: 8 January 2019; accepted: 12 March 2019

Pulmonary Circulation 2019; 9(2) 1–9
DOI: 10.1177/2045894019841987

Introduction

Pulmonary hypertension (PH) is a severe and progressive disease which results in an increase in pulmonary vascular resistance (PVR), right heart failure (RHF), and eventually death if left untreated.[1–4] Clinically, the mean pulmonary arterial pressure (mPAP) in normal adults is in the range of 10–18 mmHg. In patients with PH, mPAP values are >25 mmHg at rest and those >45mmHg at rest are diagnosed as severe PH.[5–7] It has been reported that the survival rates in patients with mPAP ≥ 42.5 mmHg are significantly lower than a similar group of patients with mPAP <42.5 mmHg,[7] with reduction in survival being a result of RHF; therefore assessment of right ventricular (RV) function is essential for the diagnosis and prognosis of PH.

The RV with its crescentic shape extends from the right atrium to the apex of the heart and forms the major portion of the anterior surface of the heart. Initially, it was described as a passive conduit for the high-volume and low-pressure pump. Subsequent studies[8–10] clearly demonstrated that a thorough understanding of RV systolic and diastolic function is critical for diagnosis and treatment of RHF and PH. RV free wall thickness (RVFWT) correlates with RV hypertrophy (RVH),[11] and RV fractional area change (RVFAC) and

Corresponding authors:
Jiwang Chen and Wei Huang, Research Resources Center, University of Illinois at Chicago, 835 S. Wolcott Avenue, MSB, Suite E102, MC937, Chicago, IL 60612, USA.
Email: chenjw@uic.edu; weihuangcq@gmail.com

tricuspid annular plane systolic excursion (TAPSE) are two parameters of RV systolic function.[12,13] Pulmonary acceleration time (PAT) and ratio of PAT/pulmonary ejection time (PET) are also two good parameters that reflect the afterload of RV.[15] Echocardiography, a non-invasive and cost-effective approach, is now commonly used in the clinical[15–18] and preclinical[19–23] realm for real-time measurement of such parameters in patients and experimental models of PH.

RV echocardiography, technically, is still challengeable for the following reasons: first, the RV is thin-walled and located immediately behind sternum, so it is difficult to image the entire RV in a single view; second, it is difficult to estimate RV volume because of its crescent shape. Despite these limitations and challenges, echocardiography remains the primary approach for the evaluation of heart functions and serves as an important predictor of survival in patients with RHF and PH.[8–10] As symptoms worsen, the RV increases in size in response to volume and pressure overload in proportion to increased PVR and right ventricular systolic pressure (RVSP). An accurate assessment of the RV function is essential to perform a complete analysis of PH.

Previous echocardiographic studies[21,23-25] in experimental models of PH are still fragmentary in terms of the evaluation of RV function. For example, Cheng et al.[21] published RV echocardiographic data including RVFAC, RV free wall thickness, PA peak velocity, PAT and PAT/PET in a mouse model of PH mediated by pulmonary artery constriction; Brittain et al.[23] reported echocardiography data (PAT, PAT/PET, cardiac output (CO), and estimate of PAP) in a mouse model of PH with a dominant negative BMPRII mutation. In these studies, there are no TAPSE data or apical four-chamber views. In addition, the animal models they used are still mild PH models and only in mice.

In this study, we performed an echocardiographic study of experimental PH, specifically focusing on RV function. We employed three commonly used rodent models of PH: a mouse model of hypoxia-mediated PH (HPH); a rat model of hypoxia + sugen 5416 (sugen); and monocrotaline (MCT)-mediated severe PH. The mouse model of HPH has been widely used to study the pathophysiology of PH and to investigate potential therapies because of transgenic features. The rat model of hypoxia + sugen-mediated PH is a severe PH model with formation of plexiform lesions,[26] which is similar to the patients with severe PAH. The rat model of MCT-mediated PH involves RHF.[27] To study RV function in these three models, we used a VEVO2100 echocardiography ultrasound system, and assessed parasternal short axis, long axis, and apical four-chamber views to examine RV structure and function.

Materials and methods

All the experimental procedures were approved by the Institutional Animal Care and Use Committee of the University of Illinois at Chicago.

Rodent models of experimental PH

In the mouse of HPH, eight-week-old male C57BL/6 mice from Charles River were exposed to hypoxia (10% O_2) in a ventilated chamber for four weeks. In two rat models of hypoxia sugen-mediated severe PH, male Sprague-Dawley rats (190–200 g) from Charles River were used. One dose of sugen (20 mg/kg) was injected into the rats subcutaneously immediately before three-week hypoxia exposure (10% O_2).[26] After hypoxia exposure, the rats were put back to the room air for another four weeks. In the MCT-induced rat PH model, rats received one dose of MCT (60 mg/kg) by intraperitoneal injection and were studied four weeks later.[28] At the end of the experiments, the animals were used for echocardiography screening and then hemodynamic measurements.

Rodent echocardiography

RV function of the three models were assessed by functional rodent echocardiography according to the procedures described previously. Briefly, the animals were anesthetized using inhaled isoflurane via a facemask and then subjected to transthoracic echo using VisualSonics Vevo 2100 (VisualSonics Inc., Toronto, ON, Canada) and two different transducers (mice: MS-550D, 22–55 MHz; rats: MS-250, 13–24 MHz). RVFAC was measured via parasternal short-axis view at mid-papillary level. RVFWT was measured during end-diastole in the parasternal short-axis mitral valve level two-dimensional (2D) or parasternal long-axis RV outflow tract level M-mode. Pulse-wave Doppler echo was used to record the pulmonary blood outflow at the level of the aortic valve in the short-axis view to measure PAT and PET. TAPSE was measured in 2D M-mode echocardiograms from the apical four-chamber view, positioning the cursor on the lateral tricuspid annulus near the free RV wall and aligning it as close as possible to the apex of the heart. Stroke volume (SV), fractional shortening (FS), ejection fraction (EF), and CO were measured from the left ventricle (LV).

Hemodynamic measurement and heart tissue histology

RVSP was determined by right heart catheterization (RHC) using a Millar pressure transducer catheter. A weight ratio of the right ventricle divided by the sum of left ventricle and septum (RV/(LV + S)) was measured to determine the extent of RVH. At the end of the experiments, the hearts were removed, washed in PBS, and fixed in 10% formalin for 48 h. The fixed hearts were cut in the short-axis direction at the middle level from apex to the base and in the same location between different groups and then processed for paraffinization. The paraffinized heart tissue sections were used for hematoxylin and eosin (H&E) staining and the images were scanned and analyzed using an Aperio ImageScope system.

Statistical analysis

Statistical analysis of experimental data was performed using GraphPad Prism 5.1 (GraphPad Software, Inc., La

Jolla, CA, USA). Results are expressed as mean ± SEM from at least three experiments. Student's t test and analysis of variance were used to compare the two or more groups, respectively. $P < 0.05$ was considered statistically significant. The correlation tests were evaluated by Pearson's test, with $r^2 > 0.75$ considered a strong correlation.

Results

In the three different rodent models of PH, VEVO2100 was used to obtain high-quality images for parasternal long-axis, short-axis, pulmonary outflow, and apical four-chamber views. M-mode tracings of LV at parasternal long-axis and data analysis are shown in Suppl. Fig. 1 and Tables 1 and 2, which demonstrate that CO significantly decrease in rat models of PH (control vs. hypoxia sugen: 78.3 ± 1.9 mL/min vs. 61.5 ± 2.6 mL/min, $P < 0.0001$; rat control vs. MCT group: 76.1 ± 3.1 mL/min vs. 63.5 ± 3.5 mL/min, $P = 0.0221$) but not in mice (normoxia vs. hypoxia: 16.1 ± 0.7 mL/min vs. 14.4 ± 3.6 mL/min, $P = 0.38$). Stroke volume significantly decreased in PH mice and rats (mouse normoxia vs. hypoxia: 32.4 ± 1.6 µL vs. 28.2 ± 0.8 µL, $P = 0.0262$; rat control vs. hypoxia sugen: 223 ± 7.3 µL vs. 184.2 ± 10.6 µL, $P = 0.0014$; rat control vs. MCT group: 217.4 ± 5.8 µL vs. 169.2 ± 11 µL, $P = 0.0031$). EF and FS did not differ significantly in either model. All the echocardiographic data were summarized in Table 1 for mouse HPH model and in Table 2 for rat hypoxia sugen and MCT PH models.

RVFAC and free wall thickness

Parasternal short-axis images of mice and rats are shown in Fig. 1a and b. According to parasternal short-axis views, we measured RVFAC at the end of diastolic and systolic phases. RVFWT was measured using M-mode of the parasternal long-axis views. RVFAC values were shown in Fig. 1c–e (mouse normoxia vs. hypoxia: 53.5 ± 3.1 vs. 20.9 ± 3.6, $P < 0.0001$; rat control vs. hypoxia sugen: 72.8 ± 3.3 vs. 38.9 ± 3.6, $P < 0.0001$; rat control vs. MCT: 71.6 ± 4.3 vs. 52.1 ± 6.7, $P = 0.0351$), with RVFWT in Fig. 1f–h (mouse normoxia vs. hypoxia: 0.32 ± 0.02 mm vs. 0.52 ± 0.01 mm, $P < 0.0001$; rat control vs. hypoxia sugen: 0.61 ± 0.02 mm vs. 1.51 ± 0.08 mm, $P < 0.0001$; rat control vs. MCT: 0.57 ± 0.03 mm vs. 1.25 ± 0.06 mm, $P < 0.0001$. In both mouse and rat models of PH, RVFAC significantly decreased but RVFWT was significantly elevated in hypertensive groups.

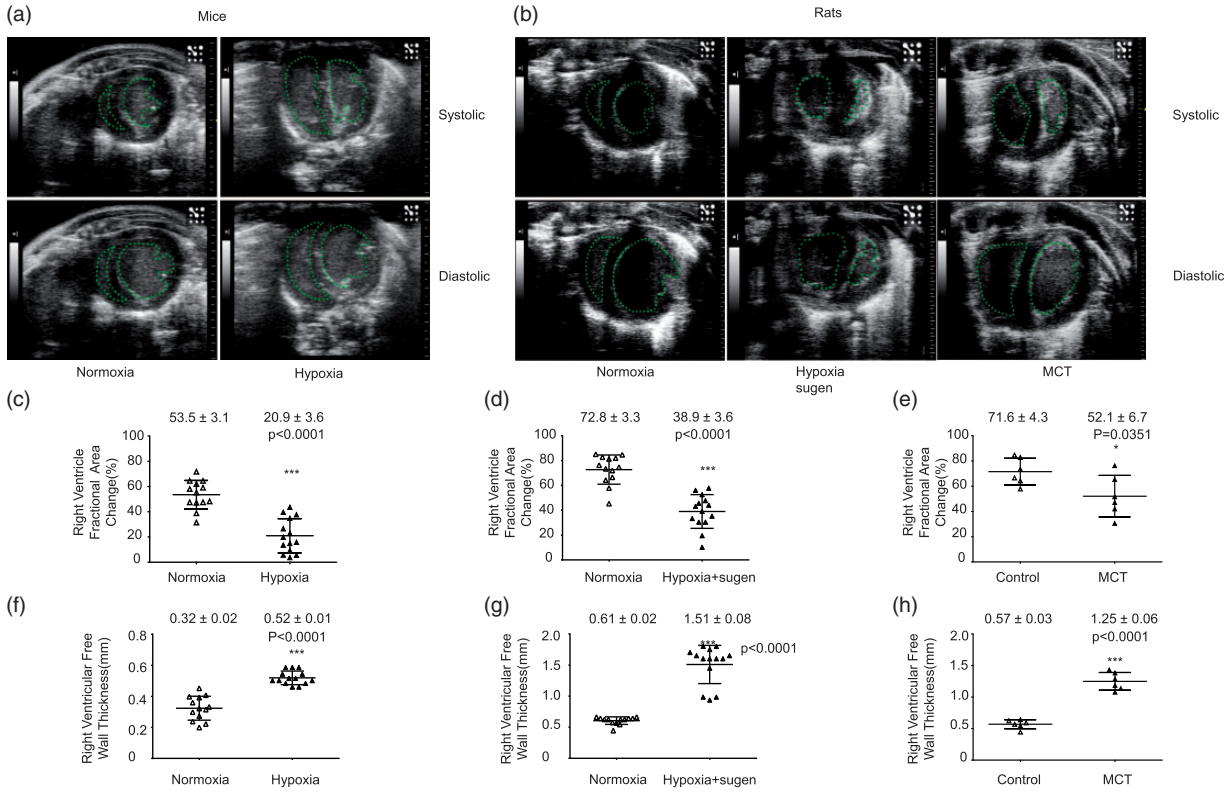

Fig. 1. RVFAC and RVFWT measured by echocardiography in a mouse model of hypoxia-mediated PH and rat model of hypoxia sugen and MCT-mediated severe PH. Parasternal short-axis views ((a) mice; (b) rats) at mid-PAP level of the left ventricle demonstrate that enlarged RV chamber at the end systole and diastole phases, decreased RVFAC and increased RVFWT, indicating decreased RV contractility and RV hypertrophy in these rodent models of PH. n ≥ 6 in each group. ***$P < 0.001$.

TAPSE

Apical four-chamber views in mice and rats are shown in Supplementary Echo Cines 1–5; these views allow visualization of the tricuspid valve. From these views, the transducer will be adjusted manually so that the tricuspid can be seen clearly. M-mode can be used to measure TAPSE. TAPSE images and quantification in the three rodent models of PH have been summarized in Fig. 2. A significant decrease of TAPSE was observed in PH models (mouse normoxia vs. hypoxia: 1.07 ± 0.06 mm vs. 0.65 ± 0.02 mm, $P < 0.0001$; rat control vs. hypoxia sugen: 2.74 ± 0.10 mm vs. 2.09 ± 0.04 mm, $P < 0.0001$; rat control vs. MCT: 2.96 ± 0.14 mm vs. 1.69 ± 0.08 mm, $P < 0.0001$.

Table 1. Echocardiographic evaluation of mice.

Mouse			
	Control	Hypoxia	*P*
RVFAC (%)	53.5 ± 3.1	20.9 ± 3.6*	<0.0001
TAPSE (mm)	1.07 ± 0.06	0.65 ± 0.02*	<0.0001
PAT (ms)	18.55 ± 0.52	11.77 ± 0.57*	<0.0001
PAT/PET	0.34 ± 0.01	0.25 ± 0.01*	<0.0001
RVFWT (mm)	0.32 ± 0.02	0.52 ± 0.01*	<0.0001
EF (%)	64.2 ± 2.4	57.0 ± 4.9	0.1785
CO (mL/min)	16.1 ± 0.7	14.4 ± 0.6	0.0829
FS (%)	28.9 ± 0.9	26.6 ± 2.2	0.3290
SV (μL)	32.4 ± 1.6	28.2 ± 0.8*	0.0262
HR (bpm)	422.8 ± 8.1	486.7 ± 15.2*	0.0012
RVSP (mmHg)	24.62 ± 0.29	31.31 ± 1.51*	0.0074
RVH	0.24 ± 0.01	0.37 ± 0.01*	<0.0001

*p<0.05, control group compared to hypoxia group.
RVFAC, right ventricle fractional area change; TAPSE, tricuspid annular plane systolic excursion; PAT, pulmonary acceleration time; PET, pulmonary ejection time; RVFWT, right ventricle free wall thickness; EF, ejection fraction; CO, cardio output; FS, fractional shortening; SV, stroke volume; HR, heart rate; RVSP, right ventricle systolic pressure; RVH, right ventricle hypertrophy.

Pulmonary acceleration time (PAT) and pulmonary ejection time (PET)

Mouse and rats pulmonary outflow images and quantification were shown in Fig. 3. PAT and PET can be measured via either parasternal long-axis or short-axis views. In mice, PAT and PAT/PET values (normoxia vs. hypoxia) are 18.55 ± 0.52 ms vs. 11.77 ± 0.57 ms, $P < 0.0001$ and 0.34 ± 0.01 vs. 0.25 ± 0.01, $P < 0.0001$, respectively; in rats, PAT and PAT/PET values (control vs. hypoxia + sugen are 30.38 ± 0.89 ms vs. 17.54 ± 0.65 ms, $P < 0.0001$ and 0.44 ± 0.02 vs. 0.22 ± 0.01, $P < 0.0001$; control vs. MCT: 27.33 ± 1.61 ms vs. 14.17 ± 0.1 ms, $P < 0.0001$ and 0.47 ± 0.02 vs. 0.2 ± 0.01, $P < 0.0001$, respectively). Both PAT and PAT/PET ratios significantly decrease in PH groups in both mice and rats.

Hemodynamic and histologic data of the heart tissues

In both mouse and rat models of PH, a Millar catheter was used to measure RVSP after echocardiography (Fig. 4). In mice, RVSP for normoxia and hypoxia group: 24.62 ± 0.29 mmHg vs. 31.31 ± 1.51 mmHg, $P = 0.0074$; in rats, RVSP for control and hypoxia sugen group: 25.90 ± 0.64 mmHg vs. 65.10 ± 3.92 mmHg, $P < 0.0001$; control

Table 2. Echocardiographic evaluation of rats.

	Rat					
	Control	Hypoxia + sugen	*P*	Control	Monocrotaline	*P*
RVFAC (%)	72.8 ± 3.3	38.9 ± 3.6*	<0.0001	71.6 ± 4.3	52.1 ± 6.7*	0.0351
TAPSE (mm)	2.74 ± 0.10	2.09 ± 0.04*	<0.0001	2.96 ± 0.14	1.69 ± 0.08*	<0.0001
PAT (ms)	30.38 ± 0.89	17.54 ± 0.65*	<0.0001	27.33 ± 1.61	14.17 ± 0.10*	<0.0001
PAT/PET	0.44 ± 0.02	0.22 ± 0.01*	<0.0001	0.47 ± 0.02	0.20 ± 0.02*	<0.0001
RVFWT (mm)	0.61 ± 0.02	1.51 ± 0.08*	<0.0001	0.57 ± 0.03	1.25 ± 0.06*	<0.0001
EF (%)	79.5 ± 1.3	74.7 ± 1.3	0.0547	80.3 ± 1.7	77.4 ± 1.4	0.2296
CO (mL/min)	78.3 ± 1.9	61.5 ± 2.6*	<0.0001	76.1 ± 3.1	63.5 ± 3.5*	0.0221
FS (%)	49.7 ± 1.5	46.5 ± 1.8	0.1815	49.5 ± 2.0	48.9 ± 3.7	0.8884
SV (μL)	223.0 ± 7.3	184.2 ± 10.6*	0.0014	217.4 ± 5.8	169.2 ± 11*	0.0031
HR (bpm)	349.7 ± 7.0	341.4 ± 4.6	0.082	373.5 ± 10.5	365.8 ± 8.5	0.0618
RVSP (mmHg)	25.09 ± 0.64	65.10 ± 3.92*	<0.0001	24.65 ± 1.24	61.87 ± 3.92*	<0.0001
RVH	0.26 ± 0.01	0.52 ± 0.02*	<0.0001	0.25 ± 0.01	0.44 ± 0.04*	0.0017

*p<0.05, control group compared to hypoxia sugen or monocrotaline group.
RVFAC, right ventricle fractional area change; TAPSE, tricuspid annular plane systolic excursion; PAT, pulmonary acceleration time; PET, pulmonary ejection time; RVFWT, right ventricle free wall thickness; EF, ejection fraction; CO, cardio output; FS, fractional shortening; SV, stroke volume; HR, heart rate; RVSP, right ventricle systolic pressure; RVH, right ventricle hypertrophy.

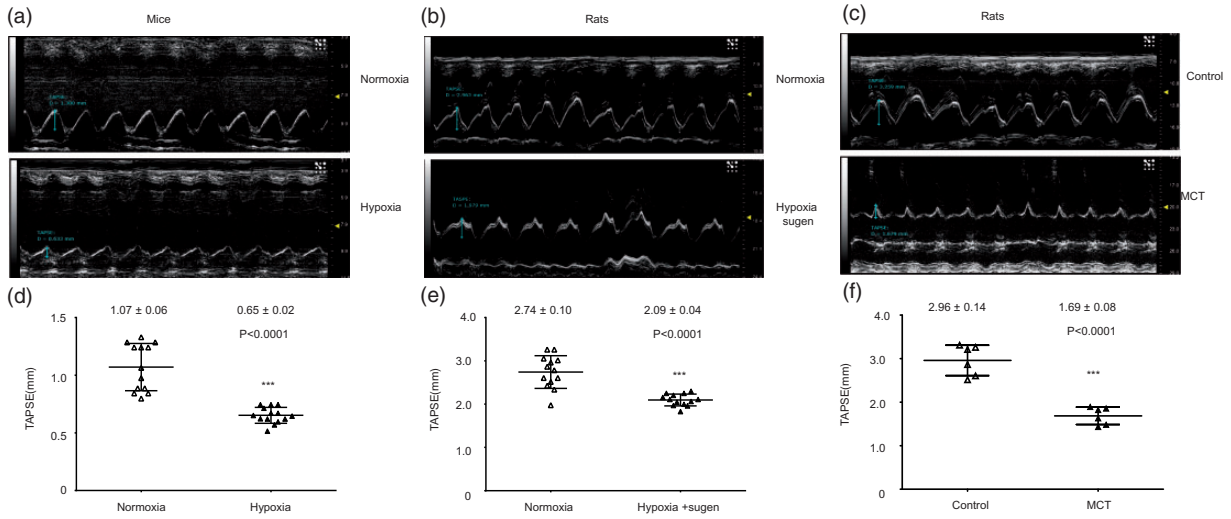

Fig. 2. Tricuspid annular plane systolic excursion (TAPSE) tracings and M-mode TAPSE data quantification in a mouse model of hypoxia-mediated PH and rat models of hypoxia surgen and and MCT mediated PH. (a, d) Mouse TAPSE tracings and TAPSE data quantification under normoxia and hypoxia exposure; (b, c, e, f) TAPSE tracings and TAPSE data quantification in control rats and hypoxia sugen-exposed rats. These data demonstrate that TAPSE decreases in these rodent models of PH, indicating decreased RV contractility in pulmonary hypertensive groups. $n \geq 6$ in each group. $^{***}P < 0.001$.

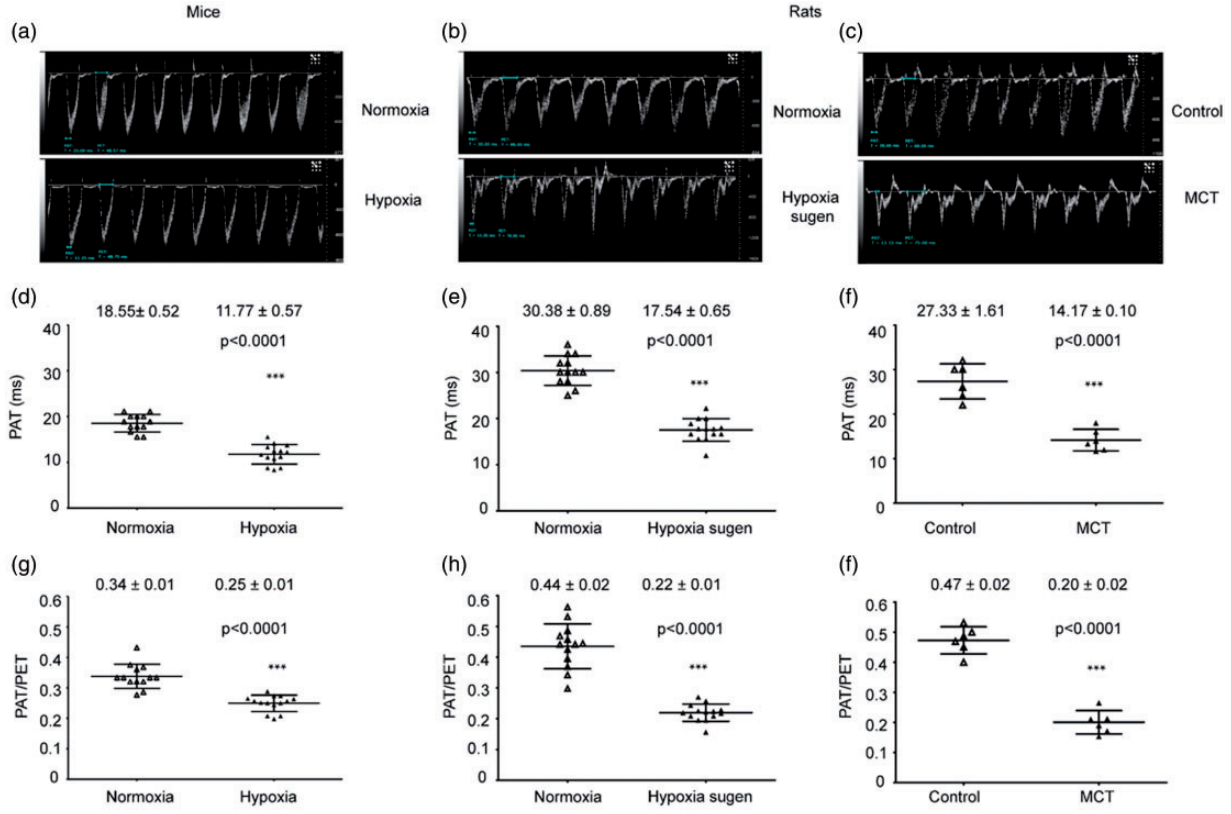

Fig. 3. Pulmonary outflow PW Doppler tracings and data quantification in mouse model of hypoxia-mediated PH and rat models of hypoxia sugen and MCT mediated PH. (a, g) Mouse PW Doppler tracings and PAT and PAT/PET ratios; (b, c, h, i) rat PW Doppler tracings and PAT and PAT/PET ratios. In both models, PAT and PAT/PET ratios significantly decrease in pulmonary hypertensive groups. $n \geq 6$ in each group. $^{***}P < 0.001$.

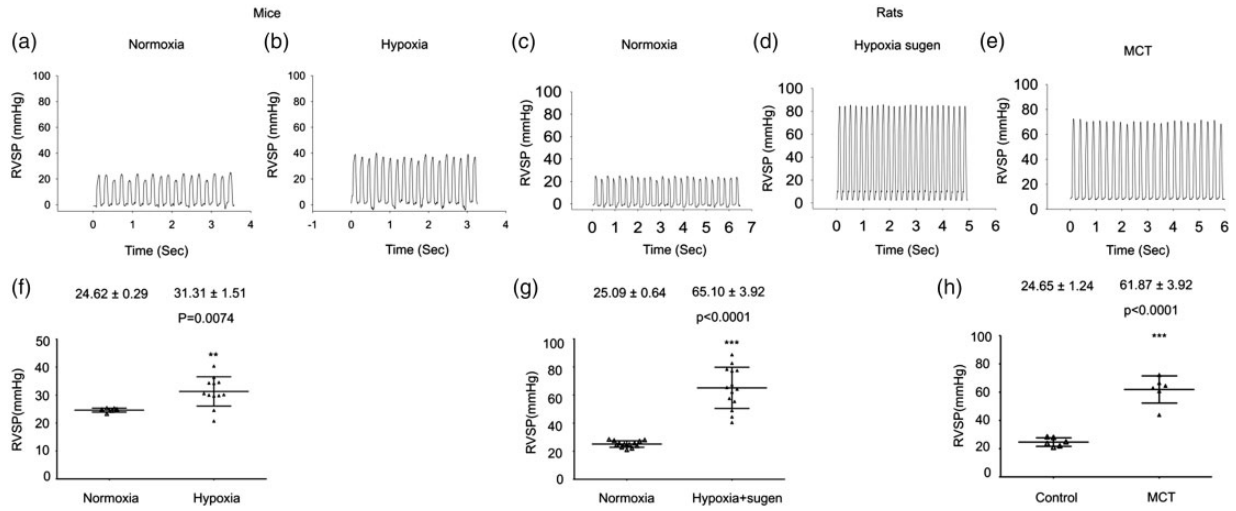

Fig. 4. RV pressure measured using a Millar catheter and RVSP data quantification in mouse and rat models of PH. (b, f) Mouse HPH tracings and RVSP data quantification; (d, e, g, h) rat HPH tracings and RVSP data quantification. RVSP values were significantly elevated in both pulmonary hypertensive mice and rats. $n \geq 6$ in each group. $^{**}P < 0.01$; $^{***}P < 0.001$.

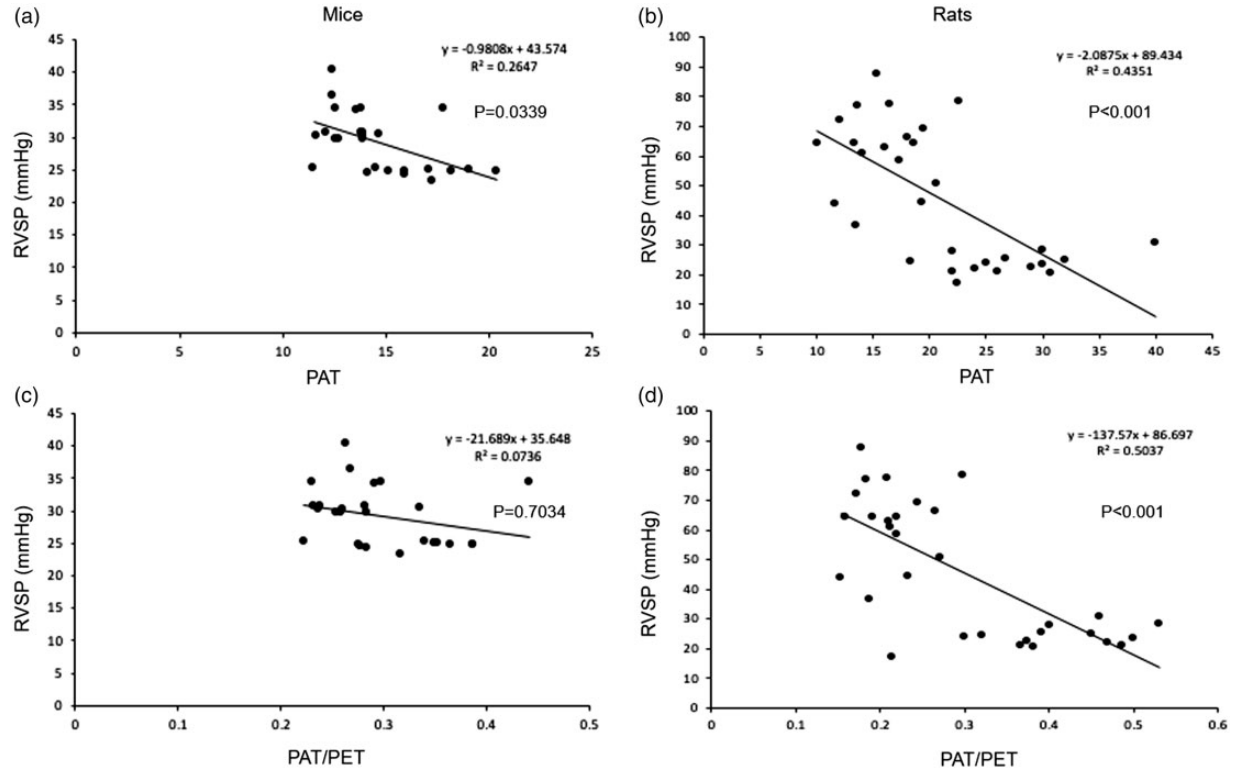

Fig. 5. Correlation between RVSP measured using a Millar catheter and PAT or PAT/PET ratios measured by echocardiography in mouse and rat models of PH. (a, c) Mouse data; (b, d) rat data. Linear correlation between RVSP and PAT or PAT/PET ratios were demonstrated. $n \geq 13$ in each group.

and MCT group: 24.65 ± 1.24 mmHg vs. 61.87 ± 3.92 mmHg, $P < 0.0001$. According to the linear regression data analysis (Fig. 5), a weak and moderated correlation was observed between RVSP and PAT or PAT/PET ratios in mouse and rat models of PH.

RVH was measured and demonstrated in Fig. 6. In mice, the ratios of RV/(LV + S) for normoxia and hypoxia group: 0.24 ± 0.01 vs. 0.37 ± 0.01, $P < 0.001$; in rats, the ratios of RV/(LV + S) for control and hypoxia sugen group: 0.26 ± 0.01 vs. 0.52 ± 0.02, $P < 0.0001$; for rat control and

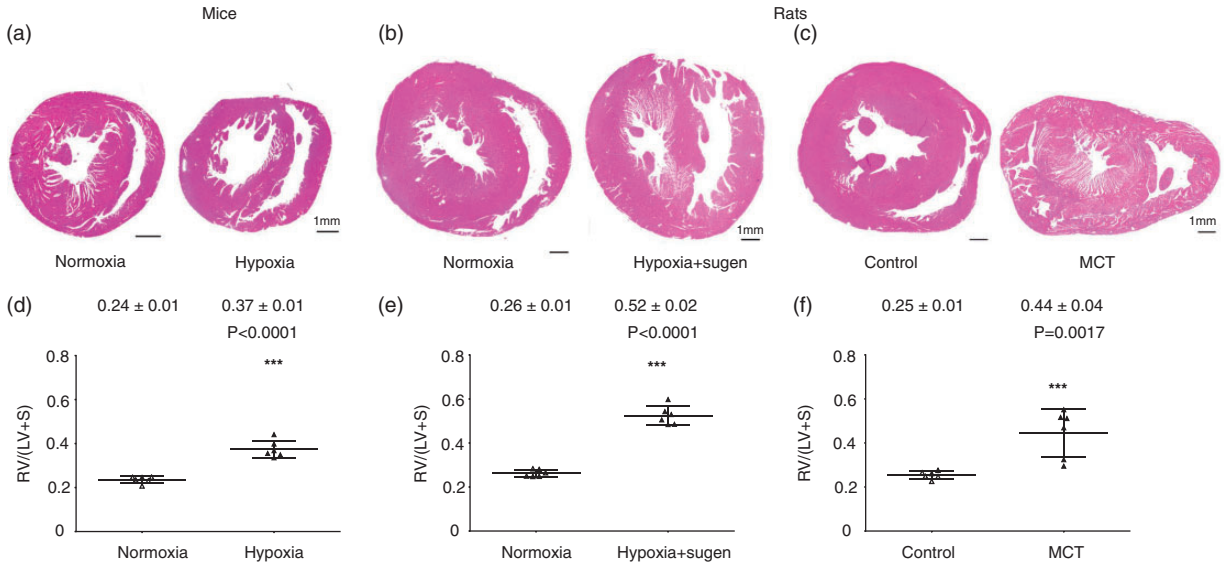

Fig. 6. Heart cross-section H&E staining and RVH data in mouse and rat models of PH. (a, d) Mouse images and RVH data; (b, c, e, f) rat images and RVH data. These images and data further confirm RVH in these rodent models of PH. n = 6 in each group. ***$P < 0.001$.

MCT group: 0.25 ± 0.01 vs. 0.44 ± 0.04, $P = 0.0017$. RVH was further confirmed by heart cross-section H&E-stained images (Fig. 6). A strong correlation was observed between RVFWT and RVH in mice ($r^2 = 0.896$, $P < 0.001$) and in rats ($r^2 = 0.774$, $P < 0.001$).

Discussion

In this study, echocardiography was employed to analyze RV function in three rodent models of PH: the mouse HPH model and the rat model of hypoxia sugen and MCT-induced severe PH. These models are widely used to study mechanisms and develop potential therapeutic strategies for PH. We demonstrated a significant decrease in RVFAC, PAT, PAT/PET ratios, TAPSE, and SV as well as dramatic elevation in RVFWT in PH models. To our understanding, this is the first reference study to examine RV function by echocardiography, RV pressure and histology in three rodent models of PH. We also presented LV echocardiography data in these models, in which we found CO significantly decreases in rat hypoxia sugen or MCT mediated PH model, but not in mouse HPH model. SV decreased in both mouse and rat models of PH in this study. Heart rates were kept constant only in rats, but significantly increased in the mice with hypoxia exposure, compared to the normoxia group (Tables 1 and 2). This explains why CO only decreased in rat models of hypoxia sugen or MCT-mediated PH.

Compared to the previous echocardiographic studies (Table S1), our echocardiographic data are consistent with these reports.[21,23–25,29–31] There are two extra unique parts in this study. First, complete TAPSE patterns were shown in these three rodent models of PH; these attribute to our capability to obtain high quality images of apical four-chamber views. Second, according to our pulmonary outflow tracings' patterns (Fig. 3), MCT and hypoxia sugen rat PH models are very similar in the patients show mid-systolic flow deceleration and notching, which is different from their controls, and very similar to patients with severe PH, whereas hypoxia alone produced tracing close to the normoxia group, only showing a single wave. These data further support that mouse HPH is a mild PH model and rat hypoxia sugen or MCT-mediated PH models are more severe.[21]

As for the possibility of estimating RVSP via echocardiography, a weak correlation between RVSP values and PAT or PAT/PET ratios were shown in mice or rats in this study (Fig. 5), although there was a trend showing lower PAT or PAT/PET values, the more severe of PH phenotypes (Fig. 3). It thus might not be accurate to estimate RVSP using PAT or PAT/PET ratios. The accurate identification of PH might be still RV catheterization.

As stated above, RV echocardiography imaging is still highly demanding. Here we provide high-quality images or cines for parasternal long-axis, short-axis, and apical four-chamber views. TAPSE tracings and data quantification (Fig. 2) have been well presented in both mouse and rat models of PH. The following important points have been suggested to ensure accurate and high-quality RV echocardiography imaging: (1) the temperature of the animal platform and the control of isoflurane outlet rate are important to keep consistent heart rate during the echo imaging and data acquisition. In general, heart rates are maintained > 400 for mice and > 300 for rats, and the animal platform temperature is kept at approximately 37 °C; (2) do not restrict to the use of the transducer holder and previously reported imaging positions, which were originally mostly designed for the hearts in stable condition. In fact, in many pathological conditions, especially after MI surgery or in severe RV hypertrophy, the positioning of the heart

may change; therefore, flexible adjustments of the transducer positioning are critically important for correct imaging; (3) accurate TAPSE images and M-mode data acquisition requires a clear apical four-chamber view; (4) RVFWT is a good parameter to evaluate RV hypertrophy because it is not affected by its neighboring right atrium and it can reflect RV diastolic and systolic functions. To accurately measure RVFWT, it is best to use the M-mode at the parasternal long-axis RV outflow tract level, which was used in this study (Suppl. Fig. 2). It can also be obtained via parasternal short-axis at mitral valve B-mode level (Supplementary Echo Cines 6–10).

There were some limitations of this study. First, in the hypoxia sugen rat PH model, we used normal healthy rats as controls for the hypoxia sugen group. To examine how sugen enhances hypoxia-mediated PH severity, the rats with hypoxia only could be another good control. Second, in this study, all mice and rats we studied were males and it is known that females have increased incidence of PH.[28,32] Third, CO and EF values were calculated from LV, not from RV. Thus, using rats with hypoxia exposure only as another control for the hypoxia sugen group, studying female animals and measuring CO and EF values from RV in these rodent models of PH may warrant our further echocardiographic studies.

In summary, we conducted a RV echocardiographic study in three rodent models of PH. RVFAC, RVFWT, PAT, and TAPSE are good parameters to evaluate RV function. Complete patterns of TAPSE and pulmonary outflow tracings were presented in these models. Thus, it can be as a reference study for the evaluation of RV functions in preclinical models of PH.

Acknowledgements

The authors thank Drs. Shamim Chowdhury, Zhiyu Dai, Liomar Neves, and Yang Song for technical support.

Conflict of interest

The author(s) declare that there is no conflict of interest.

Funding

This study was supported by the Summer Research Opportunities Program (SROP), CURA program, and the L@s GANAS Foundation at University of Illinois at Chicago. This study was partially supported by a National Natural Science Foundation (NNSF) grant 81770059.

References

1. Malenfant S, Neyron AS, Paulin R, et al. Signal transduction in the development of pulmonary arterial hypertension. *Pulm Circ* 2013; 3: 278–293.
2. Khan R, Abbasi T, Machado RF, et al. Treatment of pulmonary arterial hypertension: current and clinical trial modalities. *J Hypertens Manag* 2016; 2: 005.
3. Chen J, Sysol JR, Singla S, et al. Nicotinamide phosphoribosyltransferase promotes pulmonary vascular remodeling and is a therapeutic target for pulmonary arterial hypertension. *Circulation* 2017; 135: 1532–1546.
4. Chen J, Tang H, Sysol JR, et al. The sphingosine kinase/sphingosine-1-phosphate pathway promotes pulmonary vascular remodeling. *Am J Respir Crit Care Med* 2014; 190: 1032–1043.
5. Nauser TD and Stites S. Diagnosis and treatment of pulmonary hypertension. *Am Fam Physician* 2001; 63: 1789–1799.
6. Strange G, Playford D, Stewart S, et al. Pulmonary hypertension: prevalence and mortality in the Armadale echocardiography cohort. *Heart* 2012; 98: 1805–1811.
7. Ogawa A, Ejiri K and Matsubara H. Long-term patient survival with idiopathic/heritable pulmonary arterial hypertension treated at a single center in Japan. *Life Sci* 2014; 118: 414–419.
8. Sun JP, James KB, Yang XS, et al. Comparison of mortality rates and progression of left ventricular dysfunction in patients with idiopathic dilated cardiomyopathy and dilated versus nondilated right ventricular cavities. *Am J Cardiol* 1997; 80: 1583–1587.
9. Gavazzi A, Berzuini C, Campana C, et al. Value of right ventricular ejection fraction in predicting short-term prognosis of patients with severe chronic heart failure. *J Heart Lung Transplant* 1997; 16: 774–785.
10. De Groote P, Millaire A, Foucher-Hossein C, et al. Right ventricular ejection fraction is an independent predictor of survival in patients with moderate heart failure. *J Am Coll Cardiol* 1998; 32: 948–954.
11. Maron MS, Hauser TH, Dubrow E, et al. Right ventricular involvement in hypertrophic cardiomyopathy. *Am J Cardiol* 2007; 100(8): 1293–1298.
12. Zakaria D, Sachdeva R, Gossett JM, et al. Tricuspid annular plane systolic excursion is reduced in infants with pulmonary hypertension. *Echocardiography* 2015; 32(5): 834–838.
13. Peyrou J, Parsaï C, Chauvel C, et al. Echocardiographic assessment of right ventricular systolic function in a population of unselected patients before cardiac surgery: a multiparametric approach is necessary. *Arch Cardiovasc Dis* 2014; 107(10): 529–539.
14. Calcutteea A, Lindqvist P, Soderberg S, et al. Global and regional right ventricular dysfunction in pulmonary hypertension. *Echocardiography* 2014; 31(2): 164–171.
15. Rudski LG, Lai WW, Afilalo J, et al. Guidelines for the echocardiographic assessment of the right heart in adults: a report from the American Society of Echocardiography endorsed by the European Association of Echocardiography, a registered branch of the European Society of Cardiology, and the Canadian Society of Echocardiography. *J Am Soc Echocardiogr* 2010; 23: 685–713.
16. Parasuraman S, Walker S, Loudon BL, et al. Assessment of pulmonary artery pressure by echocardiography-A comprehensive review. *Int J Cardiol Heart Vasc* 2016; 12: 45–51.
17. Bossone E, D'Andrea A, D'Alto M, et al. Echocardiography in pulmonary arterial hypertension: from diagnosis to prognosis. *J Am Soc Echocardiogr* 2013; 26: 1–14.
18. Howard LS, Grapsa J, Dawson D, et al. Echocardiographic assessment of pulmonary hypertension: standard operating procedure. *Eur Respir Rev* 2012; 21: 239–248.
19. Ma Z, Mao L and Rajagopal S. Hemodynamic characterization of rodent models of pulmonary arterial hypertension. *J Vis Exp* 2016; 110: e53335.

20. Thibault HB, Kurtz B, Raher MJ, et al. Noninvasive assessment of murine pulmonary arterial pressure: validation and application to models of pulmonary hypertension. *Circ Cardiovasc Imaging* 2010; 3: 157–163.
21. Cheng HW, Fisch S, Cheng S, et al. Assessment of right ventricular structure and function in mouse model of pulmonary artery constriction by transthoracic echocardiography. *J Vis Exp* 2014; 84: e51041.
22. Menon RT, Shrestha AK, Reynolds CL, et al. Long-term pulmonary and cardiovascular morbidities of neonatal hyperoxia exposure in mice. *Int J Biochem Cell Biol* 2018; 94: 119–124.
23. Brittain E, Penner NL, West J, et al. Echocardiographic assessment of the right heart in mice. *J Vis Exp* 2013; 27(81).
24. Wang Y, Tian W, Xiu C, et al. Urantide improves the structure and function of right ventricle as determined by echocardiography in monocrotaline-induced pulmonary hypertension rat model. *Clin Rheumatol* 2019; 38(1): 29–35.
25. Lambert M, Boet A and Rucker-Martin C. Loss of KCNK3 is a hallmark of RV hypertrophy/dysfunction associated with pulmonary hypertension. *Cardiovasc Res* 2018; 114(6): 880–893.
26. Taraseviciene-Stewart L, Kasahara Y, Alger L, et al. Inhibition of the VEGF receptor 2 combined with chronic hypoxia causes cell death–dependent pulmonary endothelial cell proliferation and severe pulmonary hypertension. *FASEB J* 2001; 15: 427–438.
27. Zhao YD, Campbell AI, Robb M, Ng D, Stewart DJ. Protective role of angiopoietin-1 in experimental pulmonary hypertension. *Circ Res* 2003; 92: 984–991.
28. Wallace E, Morrell NW, Yang XD, et al. A sex-specific microRNA-96/5-hydroxytryptamine 1B axis influences development of pulmonary hypertension. *Am J Respir Crit Care Med* 2015; 191(12): 1432–1442.
29. Alzoubi A, Toba M and Abe K. Dehydroepiandrosterone restores right ventricular structure and function in rats with severe pulmonary arterial hypertension. *Am J Physiol Heart Circ Physiol* 2013; 304(12): H1708–1718.
30. Hargett LA, Hartman LJ, Scruggs AK, et al. Severe pulmonary arterial hypertensive rats are tolerant to mild exercise. *Pulm Circ* 2015; 5(2): 349–355.
31. Shah M, Phillips MR, Quintana M, et al. Echocardiography allows for analysis of pulmonary arterial flow in mice with congenital diaphragmatic hernia. *J Surg Res* 2018; 221: 35–42.
32. Yang YM and Sehgal PB. Smooth muscle-specific BCL6+/- knockout abrogates sex bias in chronic hypoxia-induced pulmonary arterial hypertension in mice. *Int J Endocrinol* 2018; 2018: 3473105.